Nonlinear response of interacting bosons in a quasiperiodic potential

Debamalya Dutta,[1,2] Arko Roy,[3,4] and Kush Saha[1,2]
[1]*National Institute of Science Education and Research, Jatni, Odisha 752050, India*
[2]*Homi Bhabha National Institute, Training School Complex, Anushakti Nagar, Mumbai 400094, India*
[3]*School of Physical Sciences, Indian Institute of Technology Mandi, Mandi-175075 (H.P.), India*
[4]*Pitaevskii BEC Center, CNR-INO and Dipartimento di Fisica, Università di Trento, via Sommarive 14, I-38123 Trento, Italy*

(Received 26 May 2022; revised 3 January 2023; accepted 4 January 2023; published 13 January 2023)

We theoretically study the electric pulse-driven nonlinear response of interacting bosons loaded in an optical lattice in the presence of an incommensurate superlattice potential. In the noninteracting limit ($U = 0$), the response of the localized phase differs significantly than the response of the delocalized phases. In particular, we show that the particle current contains only odd harmonics in the delocalized phase in contrast to the localized phase where both even and odd harmonics exist. The relative magnitudes of these even and odd harmonics and the contrast of the peaks can be tuned by varying frequency and the number of cycles of the applied pulse, respectively. In the presence of repulsive interactions, the amplitudes of the even and odd harmonics further depend on the relative strengths of the interaction U and the disorder potential V_0. We illustrate that the disorder and interaction-induced phases can be distinguished through the particle current. Finally, we discuss the dynamics of field-induced excitation responsible for exhibiting higher harmonics in the current spectrum.

DOI: 10.1103/PhysRevB.107.035120

I. INTRODUCTION

The unprecedented controllability of ultracold gases offers a unique test bed for verifying several condensed matter phenomena ranging from the physics of noninteracting electrons to the physics of highly correlated electrons. For example, the celebrated single-particle Anderson localization [1] of noninteracting electrons can be realized [2–6] in ultracold settings, whereas this phenomenon is difficult to observe in real materials due to suppression of disorder effect by a number of quantum phenomena [7]. The state-of-the-art ultracold atom experiments allow one to tune the atom-atom interactions to negligible value and to observe the single-atom behavior under the influence of disordered potential. This has motivated a great volume of works on ultracold bosons in the presence of disorder and weak nonlinear atom-atom interactions [8–13], revealing a plethora of intriguing collective localization phenomena [7,14–17]. Moreover, the experimental feasibility to generate quasiperiodic optical potentials presents an ideal platform to investigate another paradigmatic localization, namely Aubry-Andre localization [18] which shows localization-delocalization transition as the strength of the quasiperiodic potential is varied. Delocalization due to external driving within the Aubry-Andre model has also been studied in Refs. [19,20].

Since the atom-atom interaction can easily be tuned to strong-coupling limit using an optical lattice potential, the study of the interplay between interaction and random or quasiperiodic disorder has received much attention in recent times [21]. It has been shown that the interplay between disorder (random or quasiperiodic) and interaction leads to many-body localized (MBL) states in the highly-excited spectrum [22–26]. These many-body localized states fail to thermalize and cannot be described by the conventional statistical mechanics. It is now not a mere theoretical concept, rather a reality following an experimental evidence of the many-body localized state in a fermionic cold atomic setting [27]. Furthermore, it has been shown that the interacting bosons in the presence of both 1D and 2D random or quasiperiodic disorder exhibit a compressible insulating phase, namely Bose glass phase [28–32]. In addition, very recently the experimentally realizable quasiperiodic bosonic model has been shown to exhibit MBL-ergodic phase transition [33]. Despite several studies, the interplay between disorder and interacting bosons or fermions remains an active area of research towards investigating unconventional phases such as appearance of singular-continuous spectra, small interaction driven instabilities, anomalous transport, etc. [21,34–36].

While there are extensive studies on revealing atypical localized phases in an interacting system with quasiperiodicity at equilibrium, the response of this system to an external field has not received much attention particularly in the nonlinear regime. It is yet to be understood how different phases respond to the application of an external strong field. The reason for focusing on this particular dynamical aspect is attributed to the recent advancement of nonlinear spectroscopy stemming from the light-matter interaction which can decode the microscopic properties of interacting systems. Although this is a decades-old field and widely studied in gaseous medium [37–43], recent experimental realization of light-matter interaction in solid state systems [44,45] has renewed interest to study such effects in various quantum systems due to potential application in attosecond science. Such systems

include noninteracting Bloch solids [46–48], Mott insulators [49–52], Dirac insulators [53,54], twisted bilayer graphene [55], graphene [56], quantum spin liquids [57], quantum spin systems [58], etc. In addition, two of the authors of the present article have recently shown that the particle current in an interacting bosonic system can contain multiple odd harmonics of the applied field [59]; an effect evident in real materials.

Partly enticed by the generation of higher harmonics in our previous study on interacting bosons under synthetic electric field, and the availability of experimentally realizable quasiperiodic potential in optical lattice settings, we address here how the nonlinear response of interacting bosons to an electric pulse gets affected once we introduce quasiperiodicity. We note that recently the field driven nonlinear response has been studied in an *noninteracting* fermionic model in the presence of weak lattice potential involving disorder [60] and quasiperiodic potential [61]. However, the strong-field driven nonlinear response of an *interacting* bosonic model in the presence of a quasiperiodic disorder is yet to be addressed. We show that quasiperiodicity has dramatic effects on the nonlinear response of the different equilibrium phases of the interacting bosonic model. In the noninteracting limit, the delocalized phase exhibits only odd harmonics in contrast to the localized phase where both even and odd harmonics are illustrated. For stronger localization, the magnitude of maximum harmonic orders (i.e., cutoff) reduces for a fixed pulse frequency due to the presence of large minigaps in the system. Remarkably, we find that in the localized phase even harmonics can be further tuned by varying frequency. However, these features are absent in the delocalized phase. In the presence of interaction, the response of the field turns out to differ in the localized phase driven by interaction (Mott localization) from that of the localization due to quasiperiodicity (Aubry-Andre localization). Thus the nonlinear response may be a good probe to distinguish these two types of localization of different origins. Further, we investigate the dynamics of excitations responsible for the emergence of multiple harmonics in the system.

II. MODEL HAMILTONIAN

The time-independent Hamiltonian describing a system of one-dimensional interacting bosons loaded in optical lattices in the presence of a quasiperiodic potential is given by [20,23,29,33]

$$\hat{H} = -|J|\sum_j (c_j^\dagger c_{j+1} + \text{H.c.}) + \frac{U}{2}\sum_j n_j(n_j-1) + V_0\sum_j \cos(2\pi\alpha j) c_j^\dagger c_j, \tag{1}$$

with $|J|$ as the hopping parameter, $U > 0$ being the on-site repulsive interaction strength between the atoms, V_0 as the strength of the onsite potential, and $\alpha = (\sqrt{5}-1)/2$ being an irrational number. The bosonic creation (annihilation) operator are given by $c_j^\dagger(c_j)$ and $n_j = c_j^\dagger c_j$ is the number operator.

To study the nonlinear response, we use a n-cycle $\sin^2$ time varying potential of the form $A(t) = A_0 \sin^2(\omega t/2n)\sin(\omega t)$ with ω being the frequency of oscillation ($\omega = 2\pi n_0$), and $E(t) = -\partial_t A(t)$. The $A(t)$ *minimally* couples the system via the hopping term as $J(t) = |J|e^{i\Phi(t)}$ [49,50] with $\Phi(t) = q^* A(t) a/\hbar$, where a is the lattice constant and q^* is the effective charge of the boson [62]. We note that the particular form of the coupling is called velocity gauge and equivalent to a scalar potential term (length gauge) $E(t)\sum_j j c_j^\dagger c_j$. In fact, it is easy to show that the velocity gauge and length gauge are related by a gauge transformation [63]. With this, the effective time-dependent Hamiltonian in the velocity gauge reads as

$$\hat{H}(t) = -J(t)\sum_j (c_j^\dagger c_{j+1} + \text{H.c.}) + \frac{U}{2}\sum_j n_j(n_j-1) + V_0\sum_j \cos(2\pi\alpha j) n_j. \tag{2}$$

Note that the strength of the vector potential $A_0 \sin^2(\omega t/2n)$ smoothly varies with t and the maximum value is attained at the half-cycle of the pulse. For rest of the work, we measure A_0 in dimensionless units and n_0 in THz. It is worth mentioning here that the dynamics of harmonic generation indeed depends on the shape of the pulse as discussed in Ref. [64].

III. PARTICLE CURRENT

The response of the external time-dependent electric field is computed by employing the current operator given by

$$\hat{\mathcal{J}}(t) = -i\frac{aq^*|J|}{\hbar}\sum_j (e^{i\Phi(t)} c_j^\dagger c_{j+1} - \text{H.c.}). \tag{3}$$

We then calculate the expectation of $\hat{\mathcal{J}}(t)$ with respect to the time evolved ground state $|\Psi_0(t)\rangle$ of the Hamiltonian, i.e., $\langle\hat{\mathcal{J}}(t)\rangle = \langle\Psi_0(t)|\hat{\mathcal{J}}(t)|\Psi_0(t)\rangle$. To find $|\Psi_0(t)\rangle$, we numerically solve the time-dependent Schrödinger equation $\hat{H}(t)|\Psi_0\rangle = i\hbar\partial_t|\Psi_0\rangle$. For noninteracting Hamiltonian ($U = 0$), we use single-particle basis $|j\rangle$ to construct the Hamiltonian for system size $L = 200$ and subsequently diagonalize it to find ground state at $t = 0$. The ground state can then be written as $|\Psi_0\rangle = \sum_j a_j|j\rangle$, where a_j's are the coefficients of expansion. Note that a_js are the components of the eigenvector corresponding to the lowest eigenvalue of the system obtained through exact diagonalization (ED) [65,66]. Furthermore, $|j\rangle$ here represents the single-particle basis or the possible configurations to have 1 particle in L lattice sites. As representative examples, $|j = 1\rangle$ would mean having 1 particle in the 1st lattice site and the rest are zero. Which would translate to $|1000\cdots0\,(L\text{th lattice site})\rangle$. Similarly, $|j = 2\rangle$ would mean having 1 particle in the 2nd lattice site and the rest are zero. Which would be represented as $|0100\cdots0\,(L\text{th lattice site})\rangle$ and so on. In contrast, for $U \neq 0$, the Hamiltonian is expressed in many-particle basis, and for the current work is restricted to lattice sites of length $L = 7$ and total number of atoms $N = 7$. The dimension of the Hilbert space increases exponentially with the increase in the system size in the bosonic model, and thus computing the dynamics becomes computationally expensive. After having obtained the ground state of the interacting Hamiltonian ($U \neq 0$) at $t = 0$ employing ED, we then use fourth order Runge-Kutta algorithm with an optimum temporal step size which renders the dynamics convergent to evolve $|\Psi_0(0)\rangle$ under the effect of time-dependent Hamiltonian $\hat{H}(t)$ to find $|\Psi_0(t)\rangle$.

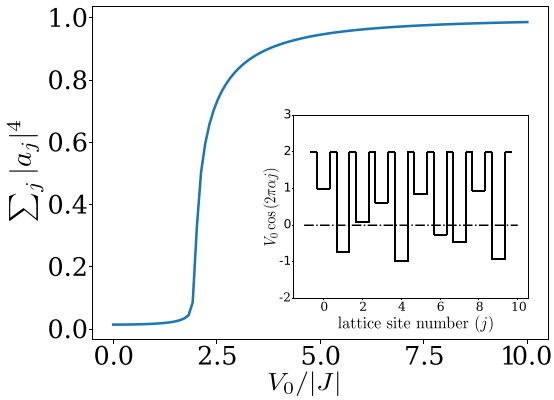

FIG. 1. Variation of IPR with scaled onsite-potential ($V_0/|J|$) diagram for noninteracting case ($U = 0$). (Inset) A schematic figure of the quasiperiodic potential with lattice site number j has been provided in inset for $V_0 = 1eV$.

With these considerations, the modulus square of the Fourier transform of $\langle \dot{\hat{\mathcal{J}}}(t) \rangle$ [the rate of change of $\langle \hat{\mathcal{J}}(t) \rangle$ with time] provides information about the intensities and frequencies ν of nonlinear excitations developed in this dynamical process. We next move on to demonstrate the effects of the time-dependent electric pulse on the noninteracting as well as the interacting Aubry-Andre model.

IV. RESULTS

A. Noninteracting case ($U = 0$)

In the noninteracting limit ($U = 0$), the model described in Eq. (1) admits delocalized (localized) phase when $V_0/|J| < 2 (V_0/|J| > 2)$, which is evident from Fig. 1 showing the variation of inverse participation ratio (IPR $= \sum_j |a_j|^4$) with the relative strength of the disordered potential.

1. Intensity spectra and underlying physical process

In the presence of $\sin^2$ pulse, the delocalized phase is identified by the appearance of only odd harmonics in the intensity spectrum of the response [see Fig. 2(a)] although the inversion symmetry of underlying Hamiltonian is broken. Notice that the order of harmonics increases with the increase in the applied field strength. The appearance of the intensity spectra with higher multiplicity of the incident frequency in the delocalized phase with $V_0 < 2|J|$ can be understood from the single-band physics with $V_0 = 0$. The intraband current for a single-band is given by $J_{\text{intra}} = n_d q v_g$, where v_g is the group velocity of the particle and n_d is the particle density. The v_g is computed as $v_g = \partial\epsilon(k)/\partial k = 2|J|a \sin(ka)$, where $\epsilon(k) = -2|J| \cos(ka)$ is the single-particle energy dispersion of Eq. (1) with $U = 0$ and $V_0 = 0$. It is to be noted in the velocity gauge, due to driving, the crystal momentum k becomes time-dependent and gets modified to $k_0 + qA(t)$. Together with $A(t)$ and k, we obtain

$$v_g(t) = 2a|J| \Bigg[\sin(k_0 a) \cos\left\{ qaA_0 \sin^2\left(\frac{\omega t}{2n}\right) \sin(\omega t) \right\} + \cos(k_0 a) \sin\left\{ qaA_0 \sin^2\left(\frac{\omega t}{2n}\right) \sin(\omega t) \right\} \Bigg]. \quad (4)$$

Figures 3(a) and 3(b) illustrate $J_{\text{intra}}(t)$ for different strength A_0 of the applied field computed using Eq. (4). Clearly, the intensity spectra $|\dot{J}_{\text{intra}}(\nu)|^2$ contains higher harmonics of applied frequency and the harmonic order increases with the field A_0 [see Figs. 3(c) and 3(d)]. We note that the analytic results are in excellent agreement with the numerical ones (red dotted line) obtained from Eq. (4) in the limit $U = 0, V_0 = 0$.

For $V_0 \neq 0$, the notion of crystal momentum is no longer valid due to the broken translation symmetry. Thus the intensity spectrum is expected to contain both even and odd harmonics. Interestingly, for $V_0 \ll 2|J|$, the intensity spectra is found to contain only odd harmonics as evident from Figs. 2(a), 2(b) and 2(e), 2(f), similar to the $V_0 = 0$ case. This feature can be explained analytically. For which we find

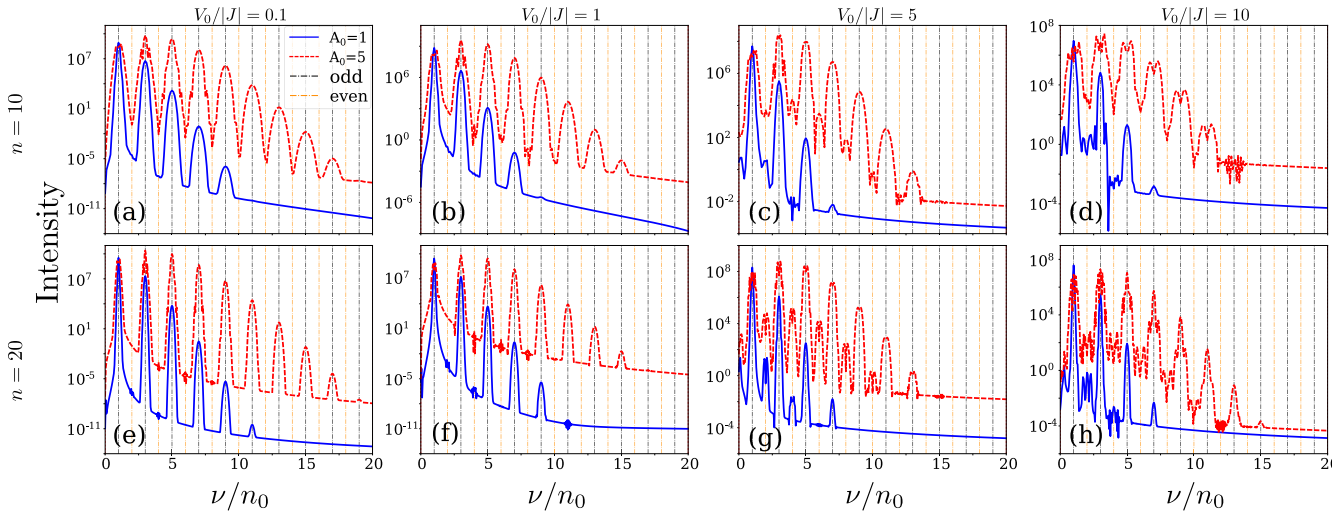

FIG. 2. Plots showing intensity spectra (the modulus square of Fourier transform of $\langle \dot{\hat{\mathcal{J}}}(t) \rangle$) with the multiplicity of incident frequency, for number of particle (N) = 1 and number of lattice sites (L) = 200 with strength of disordered potential $V_0/|J|$ and the number of cycles n as parameter.

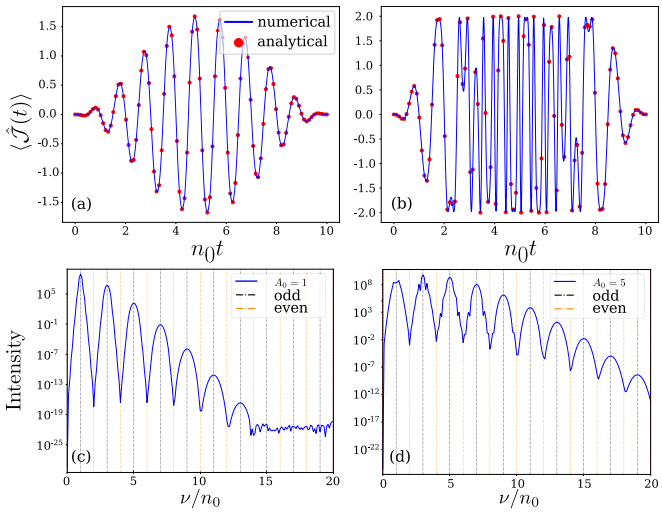

FIG. 3. (a) and (b) represent variation of $\hat{\mathcal{J}}(t)$ with time for noninteracting Bose-Hubbard model for $A_0 = 1$ and 5, respectively. (c) and (d) represent intensity spectra same as Fig. (2). The blue solid line (red dots) shows the numerical (analytical) results.

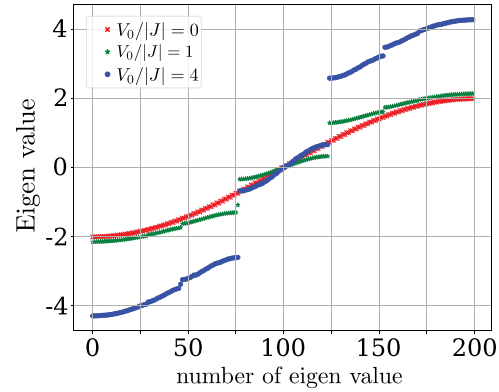

FIG. 4. Band structure of the noninteracting Hamiltonian for different strengths of disordered potential.

an approximate band dispersion relation in the presence of finite but small V_0. We treat the irrational number α as $\alpha = q_0 + h$, where q_0 is a sufficiently high-order commensurate approximation (say, $q_0 = p/q$, where p and q are integers and coprime numbers) to α, and h is a small constant. Writing the eigenstate $|\Psi\rangle$ in the single particle basis $|\Psi\rangle = \sum_j f_j c_j^\dagger |0\rangle$ as discussed in Sec. III, the eigenvalue equation $H|\Psi\rangle = E|\Psi\rangle$ leads to the standard Harper equation [67]

$$-J(f_{j+1} + f_{j-1}) + V_0 \cos(2\pi\alpha j) f_j = E f_j, \tag{5}$$

where f_j is the wave-function amplitude at site j and E is the eigenenergy. For $h = 0$, the potential becomes periodic with a period $1/q_0$ and the wave functions take the standard Bloch form, satisfying the periodic boundary condition $f_{j+q} = e^{ikq} f_j$, where $|k| \leqslant \pi/q$. Substituting $f_j = e^{ikj} u_j$ in Eq. (5) and using $u_{j+q} = u_j$, the Harper equation gives rise to an eigenvalues equation of the form $A\Phi = E\Phi$, where $\Phi = (u_1, u_2, \ldots, u_q)^T$ and A is a $q \times q$ matrix. Solving this eigenvalue equation, we obtain the characteristic polynomial $\prod_{l=1}^{q}(E - E_l(k)) = 0$, where $l = 1, 2, \ldots, q$. Thus for the commensurate potential, the extended nature of the band retains and consequently, we expect to have only odd harmonics (as shown in Appendix A).

For $h \neq 0$, hj is a slowly varying function. For simplicity, we assume it to be a small constant Q. Following the discussion in Appendix A, we obtain an eigenvalue equation as

$$-2Ju_l \cos(k + 2\pi l q_0) + V_0(u_{l+1}e^{iQ} + u_{l-1}e^{-iQ}) = E u_l, \tag{6}$$

Like earlier, this equation reduces to solving an eigenvalue equation of the form $A(Q)|\Phi|\rangle = E|\Phi\rangle$, where A now explicitly depends on Q. With a few additional steps, (detailed calculations are shown in Appendix A) we find an approximate eigenvalue equation $\prod_{l=1}^{q}\{E - E_l(k)\} + (-1)^{q-1}(\frac{V_0}{2J})^{q+1}[\cos\{(q-2)Q\} - 1] = 0$. We note that a similar calculation for constant Q and a WKB calculation for varying Q can also be found in Refs. [68–70]. For q to be a large number, the term $\mathcal{O}(V_0/2J)^q$ becomes negligibly small. Therefore the notion of Bloch band still holds even for finite but small V_0. The band structure obtained numerically as shown in Fig. 4 for a system size of $L = 200$ corroborates this as the cosine feature of the band retains except small minigaps of decreasing magnitudes. Thus the current or corresponding intensity spectrum exhibits dominant odd harmonics while the even harmonics are subdominant or negligible.

In contrast, the localized phase with $V_0 > 2|J|$ is identified by the presence of both even and odd harmonics due to strong breaking of inversion symmetry. The magnitudes of even harmonics are in general subdominant, however can be enhanced by increasing the strength of the field (A_0), frequency (ω) and the number of cycles (n) of the applied pulse. Figure 2(c) shows that the even harmonics become more amplified as we increase A_0 for a fixed ω and n. However, this feature is limited to the field strength $A_0 \lesssim V_0/|J| + 2$ [see Fig. 2(d)]. Moreover, we find that for a fixed ω and A_0, both the even and odd harmonics become much conspicuous on increasing the number of cycles n from 10 to 20 as evident from Figs. 2(e)–2(g). The origin of this feature lies in the computation of the transition matrix elements between the evolved ground state $|\Psi_0(t)\rangle$ at ($t \neq 0$) with the excited states $|f\rangle$ at the initial time $t = 0$. This particularly involves computing $\langle f|\hat{H}^{\text{int}}|\Psi_0(t)\rangle$, where $\hat{H}^{\text{int}}$ is the perturbing Hamiltonian due to the applied pulse. This turns out to be proportional to a Lorentzian in the frequency domain for a finite pulse length, that is, finite n. For $n \to \infty$, the overlap between the ground state at $t \neq 0$ with the high-lying states tends to a Dirac delta function peaking at $\nu\omega$, where ν is an integer. For a detailed calculation, we urge the reader to refer to Appendix B. Additionally, for a fixed A_0 and n, the magnitudes of even harmonics can be tuned by varying ω as shown in Fig. 5. If the pulse energy ($\hbar\omega$) is small compared to the all energy scales in the problem, the magnitudes of even harmonics are found to be negligible. As we increase ω (equivalently n_0), the magnitudes of even harmonics enhance. The reason for such behavior is due to the interband transitions involving minigaps. For small ω, the probability of interband transition is negligible. As we increase ω, the probability of interband transitions increases, and consequently, the even harmonics become much more prominent.

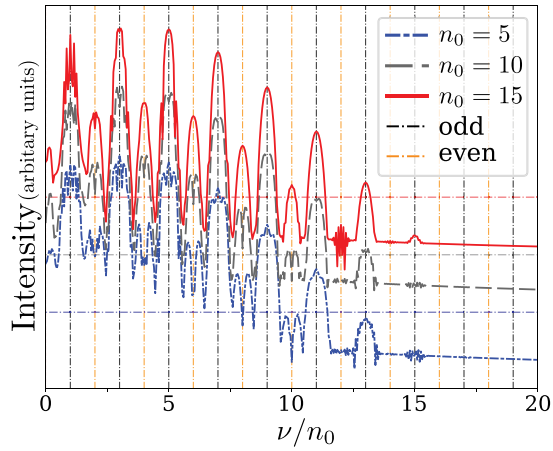

FIG. 5. Frequency dependent harmonic order for $n = 20$ cycles illustrating the enhancement in the sharpness of the even numbered peaks with the increase in frequency n_0 of the applied pulse. The y axis is in arbitrary units. The horizontal lines are the 10^0 level of respective frequency.

We complement our numerical findings of the intensity spectrum in the localized phase ($V_0 \gg 2|J|$) with a perturbative calculation. At $|J| = 0$, the Hamiltonian $\hat{H}_0 = V_0 \sum_j \cos(2\pi\alpha j) c_j^\dagger c_j$ is diagonal, and the unperturbed wave functions are localized at every site with eigenenergy $E = V_0 \cos(\alpha j)$, where j is the site index. At $V_0 \gg 2|J|$, we take $\hat{H}'(t) = |J| e^{i\Phi(t)} \sum_j (c_j^\dagger c_{j+1} + \text{H.c.})$ as time-dependent perturbation to the system. Using the standard interaction picture, the evolved ground state is obtained to be $|\Psi_0(t)\rangle_I = \hat{\mathcal{U}}_I(t,0)|\Psi_0(0)\rangle_I$, where I refers to the "interaction picture," and $\hat{\mathcal{U}}_I(t,0)$ can be obtained from $i\hbar\,\partial_t \hat{\mathcal{U}}_I(t,t_0) = \hat{H}'_I(t)\hat{\mathcal{U}}_I(t,t_0)$, where $\hat{H}'_I(t) = e^{i\frac{\hat{H}_0 t}{\hbar}} \hat{H}'(t) e^{-i\frac{\hat{H}_0 t}{\hbar}}$. For $V_0 \gg 2|J|$, $\hat{\mathcal{U}}_I(t,0)$ can be approximated as $\hat{\mathcal{U}}_I(t,0) \simeq \mathcal{I} - \frac{i}{\hbar}\int_{t_0}^{t} \hat{H}'_I(t')dt'$. Then the current in the interaction picture can be expressed as

$$\langle \hat{\mathcal{J}}(t) \rangle = {}_I\langle \psi_0(t_0)|\hat{\mathcal{U}}_I^\dagger(t,0)\hat{\mathcal{J}}_I(t)\hat{\mathcal{U}}_I(t,0)|\psi_0(t_0)\rangle_I. \quad (7)$$

Using Eq. (7), we compute current in the regime $V_0 \gg |J|$, and the corresponding plot is shown in Fig. 6. We further compare the result with the result obtained numerically using matrix diagonalization. Evidently, there is an excellent match between these two approaches.

2. *Field dependent cutoff*

We next compute field dependent cutoff frequency as demonstrated in Fig. 7. The maximum value of ν/n_0 till which the harmonic peaks appear is called the *cutoff*. In the present scenario, we find the cutoff to have a linear relationship with the strength of the vector potential A_0 as evident from Fig. 7. With the increase in A_0, the coefficients of Fourier expansion A_ν of $A(t) = \sum_\nu A_\nu e^{i\nu\omega t}$ are enhanced. Additionally, with higher ν, the magnitude of the matrix elements denoting transitions between the evolved ground states with the excited states decreases, occupying the tails of the Lorentzian and getting deviated away from the central peak value. The interplay of the product of A_ν with the magnitude of the matrix elements following the Lorentzian governs the increase of the cutoff

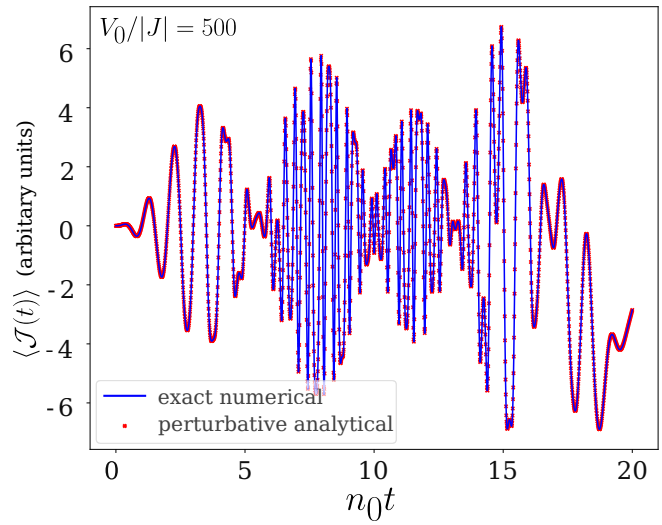

FIG. 6. Comparison between current computed using the time-dependent perturbation theory [Eq. (7)] and the exact particle current [Eq. (3)]. In the latter procedure, $|\Psi_0(t)\rangle$ has been obtained by solving the time-dependent Schrodinger equation using fourth-order Runge-Kutta method in the regime of $V_0 \gg 2|J|$. For both cases, numerical exact diagonalization techniques have been employed to compute $|\Psi_0(0)\rangle$.

with A_0. That is to say, with higher A_0, higher order Fourier coefficient A_ν begins to contribute towards the appearance of higher order peaks defining the cutoff. The detailed analytical calculation is provided in Appendix B. The introduction of the disordered onsite potential retains the linear dependence of the cutoff on the applied field as shown in Fig. 7.

B. Interacting case ($U \neq 0$)

To understand the nonlinear response of interacting bosons in the presence of quasiperiodic potential and the underlying mechanism for the generation of harmonic order, we first chart out different phases based on the

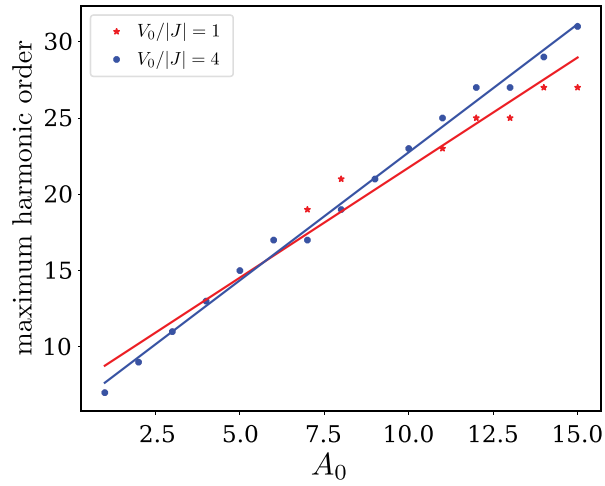

FIG. 7. Dependence of the cutoff with applied field strength in the noninteracting region.

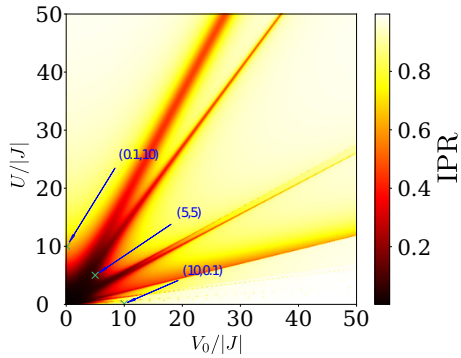

FIG. 8. False color-coded image representing the variation of IPR as a function of interaction ($U/|J|$) and onsite potential ($V_0/|J|$). The three points mark the three different cases considered in this present work.

localization properties. In doing so, we find many body ground state of the interacting Hamiltonian in Eq. (1) using exact diagonalization for system size $L = 7$ and particle number $N = 7$. This in turn leads to the computation of IPR for different parameters U and V_0 for fixed $|J|$. Figure 8 demonstrates the IPR phase diagram in the $V_0/|J| - U/|J|$ plane. We note that the phase diagram obtained from ED for system size with $L = 7$, $N = 7$ matches qualitatively well with that obtained from DMRG study with bigger system size (say, $L = 35$) as shown in Ref. [29]. Along the $V_0 = 0$ line, the standard Mott insulator-superfluid transition occurs at $U/|J| = 4$ as the IPR is around 0.25. Along the $U = 0$ line disorder driven localization-delocalization transition occurs near $V_0/|J| = 2$, corroborating the phases obtained in the noninteracting case discussed in the preceding section. For finite V_0 and U, we obtain re-entrant localized and delocalized phases depending on the values of $V_0/|J|$ and $U/|J|$ as evident from Fig. 8. The localization due to interaction turns out to differ from the disorder-induced localization as the configuration of particle distribution differs. At $t = 0$, the particle distribution is obtained using the square modulus of the coefficient ($|c_{n_{\alpha_1} n_{\alpha_2} \ldots n_{\alpha_p} \ldots}(0)|^2$) of individual many-particle basis states of the ground state wave function $|\Psi_0(t)\rangle = \sum_{n_{\alpha_1} n_{\alpha_2} \ldots n_{\alpha_p} \ldots} c_{n_{\alpha_1} n_{\alpha_2} \ldots n_{\alpha_p} \ldots}(t) |n_{\alpha_1} n_{\alpha_2} \ldots n_{\alpha_p} \ldots\rangle$, where $|n_{\alpha_1} n_{\alpha_2} \ldots n_{\alpha_p} \ldots\rangle$ denotes normalized state with n_{α_1} particles in state $|\alpha_1\rangle$, n_{α_2} particles in state $|\alpha_2\rangle, \ldots$ and $\{|\alpha_i\rangle\}$ is an orthonormal basis. The IPR is thus defined to be $\sum_{n_{\alpha_1} n_{\alpha_2} \ldots n_{\alpha_p} \ldots} |c_{n_{\alpha_1} n_{\alpha_2} \ldots n_{\alpha_p} \ldots}|^4$. For high values of $V_0/|J| \gg U/|J|$, the particles tend to accumulate in a particular site. In contrast, for $V_0/|J| \ll U/|J|$, the particles tend to be distributed equally in each site with equal density, leading to the typical Mott localization. In Table I, we provide the most probable particle distributions in lattice sites for different values of $U/|J|$ and $V_0/|J|$.

TABLE I. Most probable particle configuration in different values of $V_0/|J|$ and $U/|J|$.

$V_0/\|J\|$	$U/\|J\|$	most probable configuration
10	0.1	[0 0 0 7 0 0 0]
5	5	[2 1 0 2 0 1 1]
0.1	10	[1 1 1 1 1 1 1]

1. Intensity spectra and underlying physical process

Having discussed the possible phases, we now focus on the response of both interaction-driven localization and disorder-driven localization to the pulse field. Figure 9 represents the intensity spectra for the three representative regimes based on the probable particle configurations in Table I. Let us first focus on the $U/|J| \gg V_0/|J|$ limit (see Fig. 8), where particles are distributed equally in each lattice site. For a fixed ω and n, the interaction-driven localized phase contains only odd harmonics [Fig. 9(a)] similar to the case of delocalized phase of noninteracting Hamiltonian [Fig. 2(a)]. Interestingly, the even harmonics may emerge in this interacting regime if we vary ω and n. Figure 10 demonstrates this feature. The increase in ω indeed facilitates the substantial interband transitions for even orders within the Mott gap and quasiperiodicity-induced minigaps. The interaction however alone cannot produce even harmonics irrespective of the variation in n and ω because of the presence of inversion symmetry. This is one of the key findings of the present paper.

With $U/|J| \ll V_0/|J|$ fixing $U/|J| = 0.1$, the localization is mainly governed by the quasiperiodicity as measured through IPR given in Fig. 8, where all the particles are localized in a single site. In this case, we do not see any additional feature in the intensity pattern when compared to the completely noninteracting ($U = 0$) localized phase [see Figs. 9(c) and 10(c)]. For $U/|J| \sim V_0/|J| < 10$, the system is in delocalized phase as evident from Fig. 8. The delocalized phase in the presence of interactions seems to respond differently than the limiting cases discussed in the preceding paragraphs. In this case, even for $n = 10$-cycle pulse, we obtain comparable even and odd harmonics as evident from Fig. 9(b). As we increase the field strength, the harmonic order is enhanced. Moreover, both even and odd peaks become more prominent if we increase number of pulse cycle to $n = 20$ as clearly shown in Fig. 10(b). Thus the delocalized phase with approximately equal interaction and disorder strengths presents a completely new feature in the harmonic spectra when contrasted with the other scenario. This is another important and interesting result obtained in the present model. Additionally, we have also checked that the qualitative nature of the intensity spectra is independent of the finite size of the system. Hence the physical mechanism behind the generation of such harmonic orders would remain unaltered. This is shown in Appendix D. In the following paragraph, we investigate the role of the excited states that are responsible for giving rise to harmonic orders in different parameter regimes.

To understand the presence of harmonic orders in the current spectrum, we identify the evolved excited states that are primarily responsible for the current to contain multiple frequencies of the applied field. For $U/|J| \gg V_0/|J|$, the dynamics is governed by the Mott ground state (e.g., $|11111111\rangle$) accompanied by the contribution from all the possible excited *single dipole* states [71] where a quasiparticle-quasihole pair resides on nearest-neighbor sites such as $|1021111\rangle$ [see Figs. 11(a) and 11(d)]. When $U/|J| = V_0/|J| = 5$, that is in the interacting delocalized phase, the

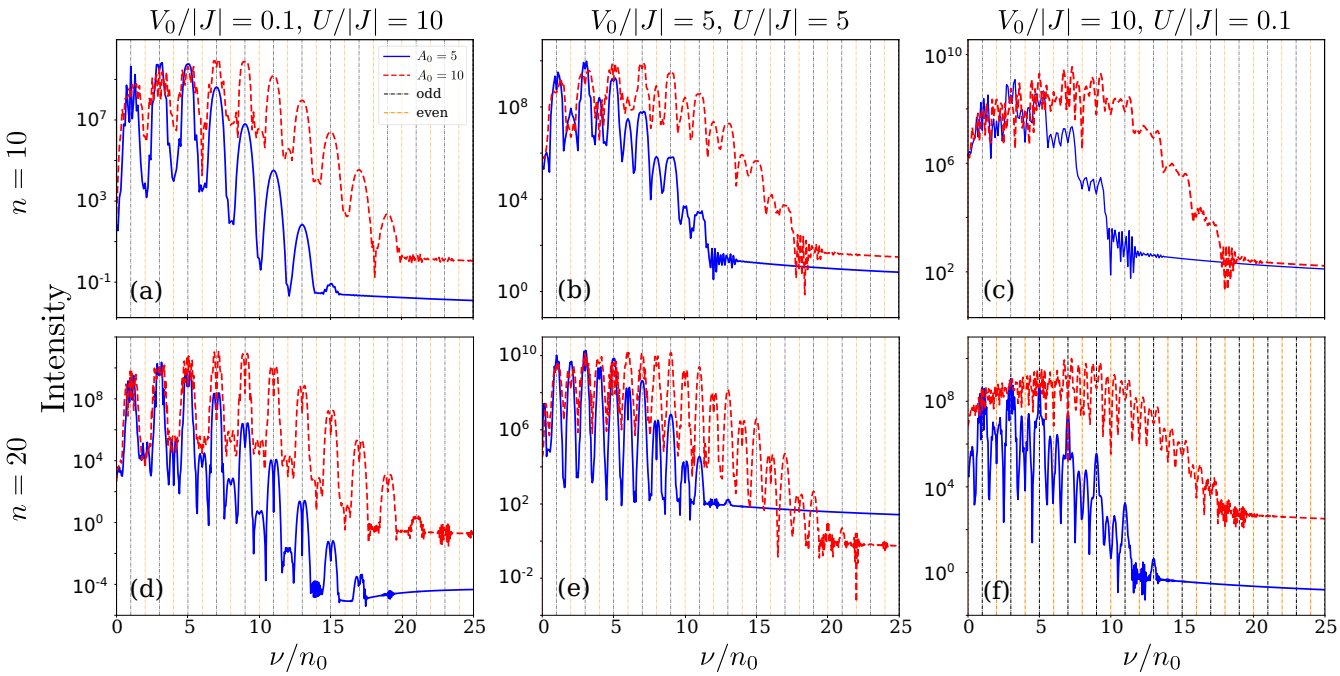

FIG. 9. Plots showing intensity spectra with the multiplicity of incident frequency, for number of particles $(N) = 7$ and number of lattice sites $(L) = 7$ for three representative points marked in the phase diagram Fig. 8. (a) $V_0/|J| = 0.1$ and $U/|J| = 10$, where the IPR ≈0.6. (b) $V_0/|J| = 5$ and $U/|J| = 5$, where the IPR ≈0.2. (c) $V_0/|J| = 10$ and $U/|J| = 0.1$, where the IPR ≈0.8 with number of cycles $n = 10$; (d), (e) and (f) show the intensity spectra for the aforementioned three points with the number of cycles $n = 20$ in the applied pulse.

contribution to current is mainly governed by the formation of single and *two dipole* states (e.g., $|1020211\rangle$); while the contribution from all other possible states is suppressed [see Figs. 11(b) and 11(e)]. On the other hand, in the deep localized phase with $V_0/|J| \gg U/|J|$ and single site occupancy, the site-localized state (nonresonant state) gives rise to higher harmonics as shown in Figs. 11(c) and 11(f).

Finally, we show in Fig. 12 the field dependent cutoff for all the parameter regimes discussed above. It turns out that the interaction does not affect the linear dependence as obtained earlier for the noninteracting case. Additionally, we find that the gradient of the cutoff decreases with increasing the strength of the disordered onsite potential V_0. This is attributed to the reduced particle current flow in the system with increasing V_0 when the particles tend to get more localized. In other words, as the minigaps increase with V_0, the probability for the interband transition reduces, leading to decrease in the cutoff frequency.

C. Model realization and experimental scope

The external electric field $E(t)$ couples to the electrons in gases and solids via a time-varying vector potential $A(t)$. On the contrary, the analogous coupling in neutral bosonic atoms happens in a synthetic manner. In particular, by modifying the mechanical momentum of the particles. Which, in experiments, can be brought about by regulating $A(t)$ through two detuned Raman lasers. The internal states of the bare atom get

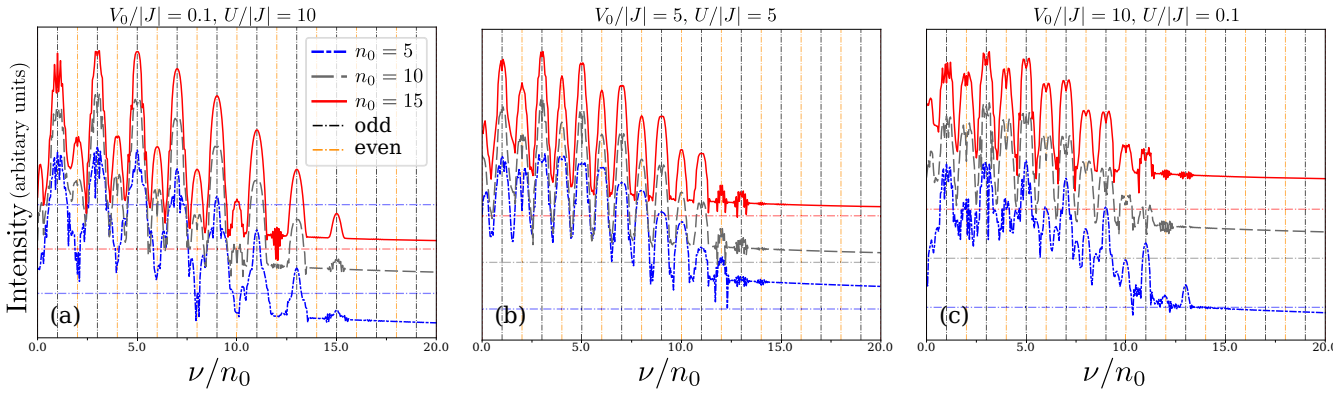

FIG. 10. Frequency dependent harmonic order for $n = 20$ cycles. Similar to Fig. 5, the plots are shifted by arbitrary y values for visual aid. The horizontal lines denote 10^0 value for their respective colors. (a) $V_0/|J| = 0.1, U/|J| = 10$, (b) $V_0/|J| = 5, U/|J| = 5$, and (c) $V_0/|J| = 10, U/|J| = 0.1$.

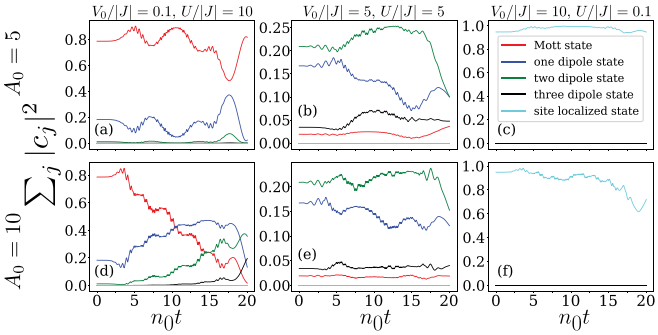

FIG. 11. Contribution of particular state $j \in$ {Mott or $1-$ or $2-$ or $3-$ dipole or site localized} states in the ensuing dynamics towards the generation of higher harmonics. (a), (b), and (c) illustrate the dynamics for $(V_0/|J| = 0.1, U/|J| = 10)$, $(V_0/|J| = 5, U/|J| = 5)$ and $(V_0/|J| = 10, U/|J| = 0.1)$ respectively with $A_0 = 5$. (d), (e), and (f) show the dynamics with similar parameters for $A_0 = 10$. Here t is measured in picoseconds.

dressed and behave like charged particles with an effective charge q^* and momentum [62]. This in turn imparts force on the dressed atoms and constitutes the underlying Hamiltonian discussed in Eq. (2) and effective particle current in Sec. 3.

We next discuss the scope and feasibility of experimental realization of higher harmonics using ultracold atoms loaded in optical lattices. Since experiments are conducted at finite temperatures, the first and foremost challenge is to achieve stable and distinct phases predicted from the zero-temperature theory as discussed in the current work. Recently, a novel and efficient way to reduce the thermal entropy of the atoms on a lattice to observe quantum phases has been devised in Ref. [72]. The particle-hole excitations can then be created in the system by a potential gradient leading to the tilting of the lattice potential [73]. The subsequent field-induced dynamics is expected to be measured in the time-of-flight experiments as illustrated in Refs. [62,74]. The dynamics of the interacting ultracold atomic rubidium sample due to the application of the femtosecond laser pulse has also been experimentally studied

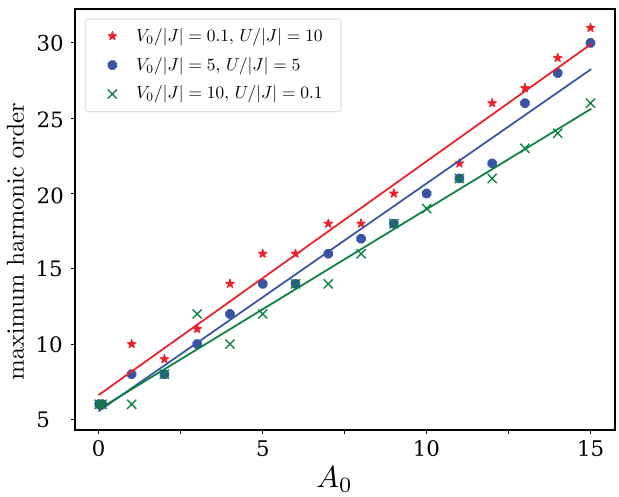

FIG. 12. Dependence of the cutoff with applied field strength in the interacting region.

recently in Ref. [75]. Thus we believe that, on one hand the possibility to experimentally observe a near ideal quantum phase and on the other, the study of strong field ionization of ultracold atoms would set the platform to study analogous generation of higher harmonics by bosons and its variants related to strong field physics in the near future.

V. CONCLUSIONS

We investigate the nonlinear response of interacting bosonic model to an electric pulse in the presence of an incommensurate potential. We find that the quasiperiodicity driven localized-delocalized phases respond differently to the electric pulse in the presence and absence of interaction. The main findings are the following: (a) in the noninteracting limit ($U = 0, V_0 \neq 0$), the delocalized phase exhibits only odd harmonics while the localized phase can contain both the even and odd harmonics and their amplitudes can be enhanced or reduced by varying the frequency of the applied field. Moreover, the cycles of the pulse can be used to sharpen the peaks of harmonic orders. (b) In the interacting case ($U \neq 0, V_0 \neq 0$), the richer physics is obtained as we tune frequency, cycles, and amplitudes of the pulse. Depending on the relative strengths of U/V_0, we can have different scenarios. i) For reasonably large interaction strength compared to the disorder potential ($U \gg V_0$), due to Mott localization, the localized Mott phase can exhibit both even and odd harmonics depending on the frequency, field strength and number of pulse cycles. This is in contrast to the disorder free interacting Mott phase discussed in Ref. [59]. (ii) Further, for comparable disorder and interaction strength ($U \simeq V_0$), the delocalized phase remarkably shows even and odd harmonics with equal magnitudes. This fact can be used as a key to distinguish it from the noninteracting delocalized ($V_0 \neq 0, U = 0$) phase. (iii) For $V_0 \gg U$, when the system is localized primarily due to disorder(Aubry-Andre localization), the even and odd harmonics can be obtained similar to the noninteracting localized phases ($U = 0, V_0 \gg 2|J|$). However, the presence of a finite but weak interaction can give rise to comparable even and odd harmonics with increasing frequency. Valid in the thermodynamic limit, our results show that in the presence of interactions, the nonlinear response can be used to distinguish Mott localization (localization driven purely by interaction) from Aubry-Andre localization (localization driven by disorder). Apart from studying the equilibrium properties, we have thus identified a possible scheme of experimental relevance concerning nonequilibrium dynamics to probe the different phases rendered by the interacting bosons in the presence of quasiperiodic disorder. The approach, based on nonlinear response of the neutral system of bosons to synthetic electric pulse provides a route towards studying high-harmonic spectroscopy and other nonlinear optical effects [76] in many-body cold-atomic systems.

ACKNOWLEDGMENTS

K.S. thanks Anamitra Mukherjee for useful discussion. D.D. acknowledges use of Virgo cluster at NISER. A.R. acknowledges the support of the Science and Engineering Research Board (SERB), Department of Science and

Technology, Government of India under the Project No. SRG/2022/000057 and IIT Mandi seed-grant funds under the Project No. IITM/SG/AR/87.

APPENDIX A: APPROXIMATE ENERGY SPECTRUM FOR $V_0 \ll 2J$ AND $U = 0$

The objective of this section is to derive an approximate energy spectrum discussed in Sec. IV A of the main text. In doing so, we substitute Eq. (5) by $f_j = e^{ikj}u_j$ and obtain

$$-J(e^{ik}u_{j+1} + e^{-ik}u_{j-1}) + V_0\cos(2\pi\alpha j)u_j = Eu_j. \quad \text{(A1)}$$

We now express the irrational number α as $\alpha = q_0 + h$, where $q_0(= p/q)$ is the rational part, and h is a small correction. In our case, $\alpha = \frac{\sqrt{5}-1}{2}$, which can be written in continued fraction expansion as

$$\frac{\sqrt{5}-1}{2} = \cfrac{1}{1+\cfrac{1}{1+\cfrac{1}{1+\cfrac{1}{1+\cfrac{1}{1+\cfrac{1}{1+\cfrac{1}{1+\cfrac{1}{1+\cdots}}}}}}}}. \quad \text{(A2)}$$

As the series continues to grow, the rational part q_0 becomes very close to α with p and q having very large values. For example, Eq. (A2) can be written in standard notation as $\frac{\sqrt{5}-1}{2} = [0; 1, 1, 1, 1, 1, 1, 1 \ldots] = 0.618033988\ldots$, where the first term 0 refers to the integer part of α. Only a few terms in the continued fraction such as $\frac{\sqrt{5}-1}{2} = [0; 1, 1, 1, 1, 1, 1, 1, 2]$ leads to rational fraction $q_0 = 34/55 = 0.618181818$. Taking a few more terms in the expansion $\frac{\sqrt{5}-1}{2} = [0; 1, 1, 1, 1, 1, 1, 1, 1, 1, 1, 1, 1, 1, 1, 1, 2]$ gives $q_0 = 987/1597 = 0.618033813$. Thus the irrational number α can be approximated by a high order commensurate number q_0 with a tiny correction term (h) as mentioned before.

For commensurate $\alpha = p/q$ ($h = 0$), $V_j = V_0\cos(2\pi\alpha j)$ is a periodic function with periodicity $R = 1/q_0$. For finite but tiny h, $2\pi hj$ is a very slowly varying number. Thus for simplicity, we treat it as a constant and denote it as Q. We note that the condition for $h \to 0$ implies q_0 is approaching to the nearest rational number of α, i.e., $q \to \infty$. Under this assumption, we express V_j in Fourier expansion as $V_j = \sum_l V_l e^{i\frac{2\pi lj}{R}}$ and similarly $u_j = \sum_l u_l e^{i\frac{2\pi lj}{R}}$.

Using the above relations, the Eq. (A1) can further be expressed as

$$-J\left(e^{ik}\sum_l u_l e^{i\frac{2\pi l(j+1)}{R}} + e^{-ik}\sum_{l'} u_{l'}e^{i\frac{2\pi l'(j-1)}{R}}\right) + \sum_l V_l e^{i\frac{2\pi lj}{R}}\sum_{l'} u_{l'}e^{i\frac{2\pi l'j}{R}} = E\sum_l u_l e^{i\frac{2\pi lja}{R}}, \quad \text{(A3)}$$

where V_l can be explicitly computed from the relation $V_l = \frac{1}{R}\sum_j e^{-i\frac{2\pi lj}{R}}V_0\cos(2\pi q_0 j + Q)$. Multiplying Eq. (A3) by $e^{-i\frac{2\pi l_1 j}{R}}$ on both sides and using the orthogonality property, we obtain

$$-J\left(e^{ik}\sum_l \delta_{ll_1}u_l e^{i\frac{2\pi l}{R}} + e^{-ik}\sum_{l'}\delta_{l'l_1}u_{l'}e^{-i\frac{2\pi l'}{R}}\right) + \sum_{ll'} V_l u_{l'}\delta_{l+l',l_1} = E\sum_{ll'} u_l\delta_{ll'}. \quad \text{(A4)}$$

It is clear from the expression of V_l, that it has only two components. For $l = 1$, $V_1 = \frac{V_0}{2}e^{iQ}$ and for $l = -1$, $V_{-1} = \frac{V_0}{2}e^{-iQ}$. Using this, Eq. (A4) can further be simplified as

$$\begin{aligned} &-J\left(e^{ik}u_l e^{i\frac{2\pi l}{R}} + e^{-ik}u_l e^{-i\frac{2\pi l}{R}}\right) \\ &+ \sum_{l'}\frac{V_0}{2}u_{l'}(\delta_{1+l',l_1}e^{iQ} + \delta_{l'-1,l_1}e^{-iQ}) = Eu_l \\ &\Rightarrow -2Ju_l\cos(k + 2\pi lq_0) + \frac{V_0}{2}(u_{l+1}e^{iQ} + u_{l-1}e^{-iQ}) \\ &= Eu_l. \end{aligned} \quad \text{(A5)}$$

Equation (A5) reduces to solving the eigenvalue equation of the form (using periodic boundary condition)

$$\begin{pmatrix} a_1' & b & 0 & 0 & \cdots & b \\ c & a_2' & b & 0 & \cdots & 0 \\ 0 & c & a_3' & b & \cdots & 0 \\ 0 & 0 & c & a_4' & \cdots & 0 \\ \vdots & \vdots & \vdots & \vdots & \ddots & \vdots \\ c & 0 & & 0 & \cdots & a_q' \end{pmatrix}_{q\times q}\begin{pmatrix} u_1 \\ u_2 \\ u_3 \\ u_4 \\ \vdots \\ u_q \end{pmatrix}_{q\times 1} = E\begin{pmatrix} u_1 \\ u_2 \\ u_3 \\ u_4 \\ \vdots \\ u_q \end{pmatrix}_{q\times 1}, \quad \text{(A6)}$$

where $a_m' = -2J\cos(k + 2\pi q_0 m)$ with $m \in Z$, $b = \frac{V_0}{2}e^{iQ}$ and $c = \frac{V_0}{2}e^{-iQ}$.

To get the energy spectrum, we need to solve the characteristic equation of Eq. (A6).

$$\begin{vmatrix} a_1 & b & 0 & 0 & \cdots & b \\ c & a_2 & b & 0 & \cdots & 0 \\ 0 & c & a_3 & b & \cdots & 0 \\ 0 & 0 & c & a_4 & \cdots & 0 \\ \vdots & \vdots & \vdots & \vdots & \ddots & \vdots \\ c & 0 & & 0 & \cdots & a_q \end{vmatrix}_{q\times q} = 0, \quad \text{(A7)}$$

where $a_m = -2J\cos(k + 2\pi q_0 m) - E$. The determinant in Eq. (A7) can further be written as the polynomial equation of the form

$$E^q + P_{q-1}E^{q-1} + P_{q-2}E^{q-2}\ldots\cdots + P_1E + P_0 = 0, \quad \text{(A8)}$$

where Ps are the coefficients of the polynomial equation containing all the parameters of Eq. (A5). However, note that the parameter Q enters in Eq. (A8) only through P_0 as $P_0 = P_0^1 + f(Q)$, where $f(Q) = (-1)^{q-1}(\lambda)^{q+1}\cos\{(q-2)Q\}$ with P_0^1 being another parameter independent of Q and $\lambda = V_0/2J$. For $Q = 0$, Eq. (A8) reduces to

$$\prod_{l=1}^{q}\{E - E_l(k)\} = 0, \quad \text{(A9)}$$

where $E_l(k)$ is the energy spectrum for the tight-binding Hamiltonian with commensurate onsite potential. For $Q \neq 0$,

Eq. (A8) transforms to

$$\prod_{l=1}^{q}\{E - E_l(k)\} + (-1)^{q-1}(\lambda)^{q+1}[\cos\{(q-2)Q\} - 1] = 0. \tag{A10}$$

APPENDIX B: TWO LEVEL MODEL AND PULSE-DRIVEN TRANSITIONS

In this section, we provide an approximate analytic expression for transition amplitudes between two states of a generic Hamiltonian in the presence of an external electromagnetic field. This will allow us to understand the presence of harmonic orders in the current discussed in the main text. We start with the Hamiltonian

$$\hat{H}_0 = \sum_i \frac{\vec{p}_i^2}{2m} + \sum_i V(r_i). \tag{B1}$$

In the presence of an external electromagnetic field, Eq. (B1) can be written as

$$\hat{H} = \sum_i \frac{(\vec{p}_i - q\vec{A}(\vec{r},t))^2}{2m} + \sum_i V(\vec{r}_i) + q\phi(\vec{r}_i,t) \tag{B2}$$

where the vector potential $\vec{A}$ and scalar potential $\phi(\vec{r},t)$ can be obtained via $\vec{E} = -\frac{\partial\vec{A}(\vec{r},t)}{\partial t}$ and $\vec{E} = -\vec{\nabla}\phi(\vec{r},t)$, respectively.

In velocity gauge, the Hamiltonian can be rewritten as

$$\hat{H}_v = \sum_i \frac{(\vec{p}_i - q\vec{A}(\vec{r}_i,t))^2}{2m} + \sum_i V(\vec{r}_i) = \hat{H}_0 + \hat{H}_v^{\text{int}}, \tag{B3}$$

where

$$H_v^{\text{int}} = \frac{1}{2m}\sum_i \big(qA(r_i,t).p_i + qp_i.A(r_i,t) + q^2A^2(r_i,t)\big). \tag{B4}$$

Using Coulomb gauge $\nabla\cdot\vec{A} = 0$ and keeping only the linear order of field strength, we find

$$H_v^{\text{int}} = \frac{2q}{2m}\sum_i A(r_j,t).p_i = -i\frac{q}{\hbar}\sum_j A(r_j,t)[r_j, H_0]. \tag{B5}$$

With this, we compute transition amplitude in the interaction picture using $\langle f|U_I(t,t_0)|i\rangle$, where $U_I(t,t_0) = \mathcal{I} + \sum_j U_I^{(j)}(t,t_0)$ and

$$U_I^{(1)}(t,t_0) = -\frac{i}{\hbar}\int_{t_0}^{t} V_I(t')dt', \tag{B6}$$

$$U_I^{(2)}(t,t_0) = -\frac{i}{\hbar}\int_{t_0}^{t} V_I(t_1)dt_1\int_{t_0}^{t_1} V_I(t_2)dt_2, \tag{B7}$$

where

$$V_I(t) = e^{iH_0t/\hbar}H_v^{\text{int}}e^{-iH_0t/\hbar}. \tag{B8}$$

For $A(r,t) = A(t) = \sum_\nu A_\nu e^{-i\nu\omega t}$, we obtain

$$\begin{aligned}
\langle f|U_I^{(1)}(t,t_0)|i\rangle &= -\frac{i}{\hbar}\int_{t_0}^{t}\langle f|V_I(t')|i\rangle dt' = -\frac{q}{\hbar^2}\int_{t_0}^{t}\sum_\nu A_\nu e^{-\nu\omega t'}e^{i(\omega_f-\omega_i)t'}\left\langle f\middle|\sum_i [r_i, H_0]\middle|i\right\rangle dt' \\
&= -\frac{q}{\hbar^2}\int_{t_0}^{t}\sum_{i,\nu} A_\nu e^{-\nu\omega t'}e^{i(\omega_f-\omega_i)t'}\langle f|(r_i.H_0 - H_0.r_i)|i\rangle dt' \\
&= -\frac{1}{\hbar}\int_{t_0}^{t}\sum_\nu A_\nu e^{-i\nu\omega t'}e^{i(\omega_f-\omega_i)t'}(\omega_f-\omega_i)\left\langle f\middle|\sum_i qr_i\middle|i\right\rangle dt' \\
&= -\frac{1}{\hbar}\int_{t_0}^{t}\sum_\nu A_\nu e^{-i\nu\omega t'}e^{i(\omega_f-\omega_i)t'}(\omega_f-\omega_i)\langle f|D|i\rangle dt'.
\end{aligned} \tag{B9}$$

If we consider that the system was in state $|i\rangle$ in deep past, i.e., $t_0 \to -\infty$ and we switch off the perturbation in far future, i.e., $t \to \infty$ compared to the dynamics of the system, the equation (B9) can be recasted as

$$\langle f|U_I^{(1)}(t,t_0)|i\rangle = -\frac{1}{\hbar}\sum_\nu A_\nu\delta(\omega_f - \omega_i - \nu\omega)(\omega_f-\omega_i)\langle f|D|i\rangle. \tag{B10}$$

Similarly,

$$\begin{aligned}
\langle f|U_I^{(2)}(t,t_0)|i\rangle &= \left(-\frac{i}{\hbar}\right)^2\left\langle f\middle|\int_{t_0}^{t} e^{iH_0t_1/\hbar}H_v^{\text{int}}(t_1)_v e^{-iH_0t_1/\hbar}dt_1\int_{t_0}^{t_1} e^{iH_0t_2/\hbar}H_v^{\text{int}}(t_2)e^{-iH_0t_2/\hbar}\middle|i\right\rangle dt_2 \\
&= \left(-\frac{i}{\hbar}\right)^2\sum_j\int_{t_0}^{t} e^{i\omega_f t_1}\sum_\nu A_\nu e^{-i\nu\omega t_1}\langle f|D|j\rangle e^{-i\omega_j t_1}dt_1(\omega_f-\omega_j)(\omega_j-\omega_i)\int_{t_0}^{t_1} e^{i\omega_j t_2} \\
&\quad\times\sum_{\nu'} A_{\nu'}e^{-i\nu'\omega t_2}\langle j|D|i\rangle e^{-\omega_i t_2}dt_2 = \left(-\frac{i}{\hbar}\right)^2\sum_j\sum_\nu\int_{t_0}^{t} A_\nu e^{i\omega_f t_1 - i\nu\omega t_1 - i\omega_j t_1}\langle f|D|j\rangle dt_1(\omega_f-\omega_j)(\omega_j-\omega_i) \\
&\quad\times\sum_{\nu'}\int_{t_0}^{t_1} A_{\nu'}e^{i\omega_j t_2 - i\omega_i t_2 - i\nu'\omega t_2}\times\langle j|D|i\rangle dt_2
\end{aligned}$$

$$= \left(-\frac{i}{\hbar}\right)^2 \sum_j \sum_\nu \int_{t_0}^{t} A_\nu e^{i\omega_f t_1 - i\nu\omega t_1 - i\omega_j t_1} \langle f|D|j\rangle dt_1 (\omega_f - \omega_j)(\omega_j - \omega_i) \sum_{\nu'} A_{\nu'} \frac{e^{i\omega_j t_2 - i\omega_i t_2 - i\nu'\omega t_2}}{i\omega_j - i\omega_i - i\nu'\omega}\Bigg|_{t_0}^{t_1} \langle j|D|i\rangle$$

$$= \left(-\frac{i}{\hbar}\right)^2 \sum_{j,\nu,\nu'} \int_{t_0}^{t} A_\nu A_{\nu'} \frac{e^{i\omega_f t_1 - i\omega_i t_1 - i\nu\omega t_1 - i\nu'\omega t_1}}{i\omega_j - i\omega_i - i\nu'\omega} dt_1 (\omega_f - \omega_j)(\omega_j - \omega_i) \langle f|D|j\rangle\langle j|D|i\rangle$$

$$= \left(-\frac{i}{\hbar}\right)^2 \sum_{j,\nu,\nu'} \int_{t_0}^{t} A_\nu A_{\nu'} \frac{e^{i\omega_f t_1 - i\omega_i t_1 - i\nu\omega t_1 - i\nu'\omega t_1}}{i\omega_j - i\omega_i - i\nu'\omega} dt_1 (\omega_f - \omega_j)(\omega_j - \omega_i) \langle f|D|j\rangle\langle j|D|i\rangle$$

$$= \left(-\frac{i}{\hbar}\right)^2 \sum_{j,\nu,\nu'} A_\nu A_{\nu'} \frac{\delta(\omega_f - \omega_i - (\nu+\nu')\omega)}{i\omega_j - i\omega_i - i\nu'\omega} (\omega_f - \omega_j)(\omega_j - \omega_i) \langle f|D|j\rangle\langle j|D|i\rangle. \tag{B11}$$

In a similar way, it is easy to find $\langle f|U_I^{(3)}(t,t_0)|i\rangle$ contains $\delta(\omega_f - \omega_i - (\nu+\nu'+\nu'')\omega)$ and higher orders as well. If the external field contain only one Fourier component, e.g., $\nu = 1$, then the transition amplitude is nonzero only when $\omega_f - \omega_i = \omega$, $\omega_f - \omega_i = 2\omega$, $\omega_f - \omega_i = 3\omega$, and so on.

Thus for the incident light with lower frequency than the energy difference between the two eigenstates, the transition amplitude, $P = |\langle f|U_I(t,t_0)|i\rangle|^2$ can contain multiple frequencies of the incident light, provided that the process should be adiabatic or slow enough compared to the dynamics of the system. The process is typically called the multiphoton process.

APPENDIX C: PERTURBATIVE CURRENT EXPRESSION FOR $V_0 \gg 2J$

In this section, we derive perturbative expressions for the current discussed in section IV of the main text. We treat $H_0 = V_0 \sum_j \cos(2\pi\alpha j) c_j^\dagger c_j$ as the nonperturbative Hamiltonian and $\hat{H}'(t) = |J| e^{i\Phi(t)} \sum_j c_{j+1}^\dagger c_j + h.c$ as the perturbation. To use time-dependent perturbation in the interaction picture, we define

$$|\psi(t)\rangle_I = e^{i\frac{\hat{H}_0 t}{\hbar}} |\psi(t)\rangle_S, \tag{C1}$$

where I and S denote the interaction and Schrodinger picture, respectively. Equation (C1), leads to the equation

$$i\hbar \frac{\partial |\psi(t)\rangle_I}{\partial t} = \hat{H}'_I(t)|\psi(t)\rangle_I, \tag{C2}$$

where $H'_I(t) = e^{-i\frac{\hat{H}_0 t}{\hbar}} H'(t) e^{i\frac{\hat{H}_0 t}{\hbar}}$. Then the time evolution of state vector is can be written as

$$|\psi(t)\rangle_I = \hat{\mathcal{U}}_I(t,t_0)|\psi(t_0)\rangle_I, \tag{C3}$$

which follows the differential equation $i\hbar \frac{\partial \hat{\mathcal{U}}_I(t,t_0)}{\partial t} = \hat{H}'_I(t)\hat{\mathcal{U}}_I(t,t_0)$, where t_0 is the initial time of the perturbation.

Keeping only the first term in the expansion of $\hat{\mathcal{U}}_I(t,t_0)$, the evolved state reads as

$$|\psi(t)\rangle_I = \left(\mathcal{I} - \frac{i}{\hbar}\int_{t_0}^{t} \hat{H}'_I(t')dt'\right)|\psi(t_0)\rangle_I. \tag{C4}$$

With this, the expectation of the current operator can be expressed as

$$\begin{aligned}\langle \hat{\mathcal{J}}(t)\rangle &= {}_S\langle\psi_0(t)|\hat{\mathcal{J}}_S(t)|\psi_0(t)\rangle_S \\ &= {}_S\langle\psi_0(t)|e^{-i\frac{\hat{H}_0 t}{\hbar}} e^{i\frac{\hat{H}_0 t}{\hbar}} \hat{\mathcal{J}}_S(t) e^{-i\frac{\hat{H}_0 t}{\hbar}} e^{i\frac{\hat{H}_0 t}{\hbar}} |\psi_0(t)\rangle_S \\ &= {}_I\langle\psi_0(t)|\hat{\mathcal{J}}_I(t)|\psi_0(t)\rangle_I \\ &= {}_I\langle\psi_0(t_0)|\left(\mathcal{I} + \frac{i}{\hbar}\int_{t_0}^{t} \hat{H}'_I(t')dt'\right)\hat{\mathcal{J}}_I(t) \\ &\quad \times \left(\mathcal{I} - \frac{i}{\hbar}\int_{t_0}^{t} \hat{H}'_I(t')dt'\right)|\psi_0(t_0)\rangle_I,\end{aligned} \tag{C5}$$

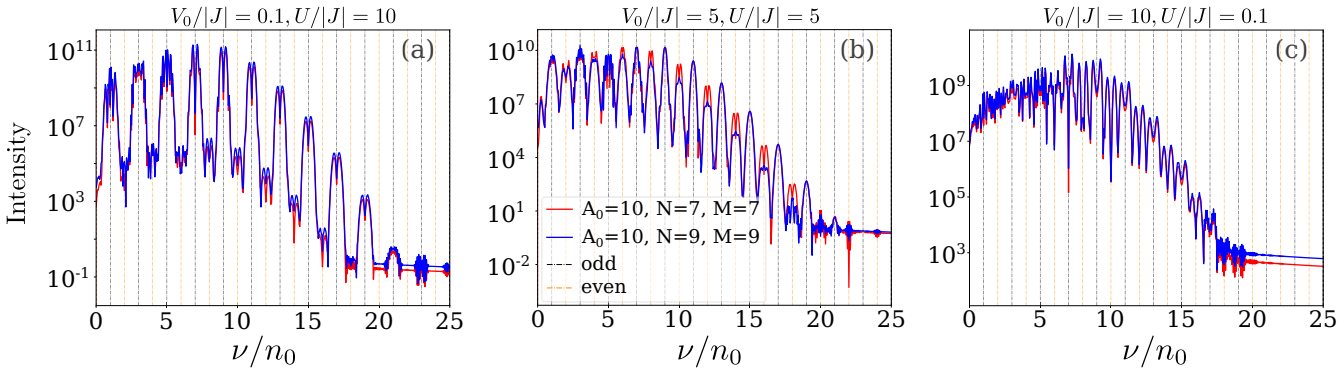

FIG. 13. Plots showing a comparison of intensity spectra with the multiplicity of incident frequency, for the number of particles $(N) = 7$ and the number of lattice sites $(L) = 7$, with the number of particles $(N) = 9$ and the number of lattice sites $(L) = 9$ in three representative points marked in the phase diagram Fig 8. (a) $V_0/|J| = 0.1$ and $U/|J| = 10$, where the IPR ≈0.6. (b) $V_0/|J| = 5$ and $U/|J| = 5$, where the IPR ≈0.2. (c) $V_0/|J| = 10$ and $U/|J| = 0.1$, where the IPR ≈0.8 with the number of cycles $n = 20$ and $A_0 = 10$.

where $|\psi_0(t_0)\rangle_S$ can be obtained by diagonalizing the full $\hat{H}(t_0)$.

APPENDIX D: DEPENDENCE ON SYSTEM SIZE

Here, we present additional results to justify that our calculations are devoid of any finite size effects. In Fig. 13, we compare intensity spectra between two different system sizes: (i) 7 particles and 7 sites and (ii) 9 particles and 9 sites, for all three distinct phases discussed in the main text. Interestingly, the results of (i) match reasonably well with the results of (ii). We note that going beyond the configuration with 9 particles and 9 sites for exact diagonalization (ED) is computationally expensive. We further point out that the generation of intensity spectra in the interacting case is not mean-field in nature; therefore, to describe it, one requires a full diagonalization of the system. This restricts the system sizes that we could access due to the exponential growth of the Hilbert space. We would also like to point out that there exist further works using exact diagonalization [66,77] (and complementing it with the density matrix renormalization group (DMRG) Ref. [78]) in the bosonic model, where also convergence seems to be achieved within similar system sizes revealing qualitatively identical physics. Thus we strongly believe that our results will be valid in the thermodynamic limit.

[1] P. W. Anderson, Phys. Rev. **109**, 1492 (1958).
[2] J. Billy, V. Josse, Z. Zuo, A. Bernard, B. Hambrecht, P. Lugan, D. Clément, L. Sanchez-Palencia, P. Bouyer, and A. Aspect, Nature (London) **453**, 891 (2008).
[3] G. Roati, C. D'Errico, L. Fallani, M. Fattori, C. Fort, M. Zaccanti, G. Modugno, M. Modugno, and M. Inguscio, Nature (London) **453**, 895 (2008).
[4] S. S. Kondov, W. R. McGehee, J. J. Zirbel, and B. DeMarco, Science **334**, 66 (2011).
[5] F. Jendrzejewski, A. Bernard, K. Müller, P. Cheinet, V. Josse, M. Piraud, L. Pezzé, L. Sanchez-Palencia, A. Aspect, and P. Bouyer, Nat. Phys. **8**, 398 (2012).
[6] D. H. White, T. A. Haase, D. J. Brown, M. D. Hoogerland, M. S. Najafabadi, J. L. Helm, C. Gies, D. Schumayer, and D. A. W. Hutchinson, Nat. Commun. **11**, 4942 (2020).
[7] L. Fallani, C. Fort, and M. Inguscio, Adv. At. Mol. Opt. Phys. **56**, 119 (2008).
[8] M. Larcher, F. Dalfovo, and M. Modugno, Phys. Rev. A **80**, 053606 (2009).
[9] M. Modugno, New J. Phys. **11**, 033023 (2009).
[10] B. Deissler, M. Zaccanti, G. Roati, C. D'Errico, M. Fattori, and M. a. Modugno, Nat. Phys. **6**, 354 (2010).
[11] M. Larcher, M. Modugno, and F. Dalfovo, Phys. Rev. A **83**, 013624 (2011).
[12] E. Lucioni, B. Deissler, L. Tanzi, G. Roati, M. Zaccanti, M. Modugno, M. Larcher, F. Dalfovo, M. Inguscio, and G. Modugno, Phys. Rev. Lett. **106**, 230403 (2011).
[13] M. Larcher, T. V. Laptyeva, J. D. Bodyfelt, F. Dalfovo, M. Modugno, and S. Flach, New J. Phys. **14**, 103036 (2012).
[14] V. Gurarie, G. Refael, and J. T. Chalker, Phys. Rev. Lett. **101**, 170407 (2008).
[15] P. Lugan and L. Sanchez-Palencia, Phys. Rev. A **84**, 013612 (2011).
[16] S. Lellouch, L.-K. Lim, and L. Sanchez-Palencia, Phys. Rev. A **92**, 043611 (2015).
[17] P. Lugan, D. Clément, P. Bouyer, A. Aspect, and L. Sanchez-Palencia, Phys. Rev. Lett. **99**, 180402 (2007).
[18] S. Aubry and G. André, Ann. Israel Phys. Soc. **3**, 133 (1980).
[19] S. Ray, A. Ghosh, and S. Sinha, Phys. Rev. E **97**, 010101(R) (2018).
[20] S. Ray, S. Sinha, and K. Sengupta, Phys. Rev. A **98**, 053631 (2018).
[21] Y. Yoo, J. Lee, and B. Swingle, Phys. Rev. B **102**, 195142 (2020).
[22] D. Basko, I. Aleiner, and B. Altshuler, Ann. Phys. **321**, 1126 (2006).
[23] S. Iyer, V. Oganesyan, G. Refael, and D. A. Huse, Phys. Rev. B **87**, 134202 (2013).
[24] A. Pal and D. A. Huse, Phys. Rev. B **82**, 174411 (2010).
[25] A. C. Potter, R. Vasseur, and S. A. Parameswaran, Phys. Rev. X **5**, 031033 (2015).
[26] M. Serbyn, Z. Papić, and D. A. Abanin, Phys. Rev. X **5**, 041047 (2015).
[27] P. Bordia, H. Lüschen, U. Schneider, M. Knap, and I. Bloch, Nat. Phys. **13**, 460 (2017).
[28] M. P. A. Fisher, P. B. Weichman, G. Grinstein, and D. S. Fisher, Phys. Rev. B **40**, 546 (1989).
[29] G. Roux, T. Barthel, I. P. McCulloch, C. Kollath, U. Schollwöck, and T. Giamarchi, Phys. Rev. A **78**, 023628 (2008).
[30] H. Yao, T. Giamarchi, and L. Sanchez-Palencia, Phys. Rev. Lett. **125**, 060401 (2020).
[31] M. Ciardi, T. Macrì, and F. Cinti, Phys. Rev. A **105**, L011301 (2022).
[32] M. Ciardi, T. Macrì, and F. Cinti, Entropy **24**, 265 (2022).
[33] A. Dutta, S. Mukerjee, and K. Sengupta, Phys. Rev. B **98**, 144205 (2018).
[34] Y. B. Lev, D. M. Kennes, C. Klöckner, D. R. Reichman, and C. Karrasch, Europhys. Lett. **119**, 37003 (2017).
[35] D. J. Luitz, N. Laflorencie, and F. Alet, Phys. Rev. B **91**, 081103(R) (2015).
[36] T. Kohlert, S. Scherg, X. Li, H. P. Lüschen, S. Das Sarma, I. Bloch, and M. Aidelsburger, Phys. Rev. Lett. **122**, 170403 (2019).
[37] M. Ferray, A. L. Huillier, X. F. Li, L. A. Lompre, G. Mainfray, and C. Manus, J. Phys. B: At., Mol. Opt. Phys. **21**, L31 (1988).
[38] A. L'Huillier, K. J. Schafer, and K. C. Kulander, Phys. Rev. Lett. **66**, 2200 (1991).
[39] J. L. Krause, K. J. Schafer, and K. C. Kulander, Phys. Rev. A **45**, 4998 (1992).
[40] J. L. Krause, K. J. Schafer, and K. C. Kulander, Phys. Rev. Lett. **68**, 3535 (1992).
[41] J. J. Macklin, J. D. Kmetec, and C. L. Gordon, Phys. Rev. Lett. **70**, 766 (1993).
[42] A. L'Huillier and P. Balcou, Phys. Rev. Lett. **70**, 774 (1993).

[43] M. Lewenstein, P. Balcou, M. Y. Ivanov, A. L'Huillier, and P. B. Corkum, Phys. Rev. A **49**, 2117 (1994).
[44] S. Ghimire, A. D. DiChiara, E. Sistrunk, P. Agostini, L. F. DiMauro, and D. A. Reis, Nat. Phys. **7**, 138 (2011).
[45] S. Ghimire, A. D. DiChiara, E. Sistrunk, G. Ndabashimiye, U. B. Szafruga, A. Mohammad, P. Agostini, L. F. DiMauro, and D. A. Reis, Phys. Rev. A **85**, 043836 (2012).
[46] S. Ghimire and D. A. Reis, Nat. Phys. **15**, 10 (2019).
[47] C. Yu, S. Jiang, and R. Lu, Adv. Phys.: X **4**, 1562982 (2019).
[48] M. Wu, S. Ghimire, D. A. Reis, K. J. Schafer, and M. B. Gaarde, Phys. Rev. A **91**, 043839 (2015).
[49] R. Silva, I. V. Blinov, A. N. Rubtsov, O. Smirnova, and M. Ivanov, Nat. Photonics **12**, 266 (2018).
[50] Y. Murakami and P. Werner, Phys. Rev. B **98**, 075102 (2018).
[51] Y. Murakami, S. Takayoshi, A. Koga, and P. Werner, Phys. Rev. B **103**, 035110 (2021).
[52] Y. Murakami, K. Uchida, A. Koga, K. Tanaka, and P. Werner, Phys. Rev. Lett. **129**, 157401 (2022).
[53] B. Cheng, N. Kanda, T. N. Ikeda, T. Matsuda, P. Xia, T. Schumann, S. Stemmer, J. Itatani, N. P. Armitage, and R. Matsunaga, Phys. Rev. Lett. **124**, 117402 (2020).
[54] H. Taya, M. Hongo, and T. N. Ikeda, Phys. Rev. B **104**, L140305 (2021).
[55] T. N. Ikeda, Phys. Rev. Res. **2**, 032015 (2020).
[56] M. S. Mrudul and G. Dixit, Phys. Rev. B **103**, 094308 (2021).
[57] M. Kanega, T. N. Ikeda, and M. Sato, Phys. Rev. Res. **3**, L032024 (2021).
[58] T. N. Ikeda and M. Sato, Phys. Rev. B **100**, 214424 (2019).
[59] A. Roy, S. Bera, and K. Saha, Phys. Rev. Res. **2**, 043133 (2020).
[60] K. Chinzei and T. N. Ikeda, Phys. Rev. Res. **2**, 013033 (2020).
[61] A. Pattanayak, A. Jiménez-Galán, M. Ivanov, and G. Dixit, arXiv:2101.08536.
[62] Y.-J. Lin, R. L. Compton, K. Jiménez-García, W. D. Phillips, J. V. Porto, and I. B. Spielman, Nat. Phys. **7**, 531 (2011).
[63] J. B. Krieger and G. J. Iafrate, Phys. Rev. B **33**, 5494 (1986).
[64] E. G. Neyra, P. Vaveliuk, E. Pisanty, A. S. Maxwell, M. Lewenstein, and M. F. Ciappina, Phys. Rev. A **103**, 053124 (2021).
[65] D. Raventós, T. Graß, M. Lewenstein, and B. Juliá-Díaz, J. Phys. B: At., Mol. Opt. Phys. **50**, 113001 (2017).
[66] J. M. Zhang and R. X. Dong, Eur. J. Phys. **31**, 591 (2010).
[67] P. G. Harper, Proc. Phys. Soc. Sect. A **68**, 879 (1955).
[68] M. Y. Azbel, Phys. Rev. Lett. **43**, 1954 (1979).
[69] J. B. Sokoloff, Phys. Rev. B **23**, 2039 (1981).
[70] J. B. Sokoloff, Phys. Rev. B **23**, 6422 (1981).
[71] S. Sachdev, K. Sengupta, and S. M. Girvin, Phys. Rev. B **66**, 075128 (2002).
[72] B. Yang, H. Sun, C.-J. Huang, H.-Y. Wang, Y. Deng, H.-N. Dai, Z.-S. Yuan, and J.-W. Pan, Science **369**, 550 (2020).
[73] M. Greiner, O. Mandel, T. Esslinger, T. W. Hansch, and I. Bloch, Nature (London) **415**, 39 (2002).
[74] J. Dalibard, F. Gerbier, G. Juzeliūnas, and P. Öhberg, Rev. Mod. Phys. **83**, 1523 (2011).
[75] P. Wessels, B. Ruff, T. Kroker, A. K. Kazansky, N. M. Kabachnik, K. Sengstock, M. Drescher, and J. Simonet, Commun. Phys. **1**, 32 (2018).
[76] R. W. Boyd, *Nonlinear Optics*, 4th ed., edited by R. W. Boyd (Academic Press, 2020).
[77] D. Jaksch, C. Bruder, J. I. Cirac, C. W. Gardiner, and P. Zoller, Phys. Rev. Lett. **81**, 3108 (1998).
[78] U. Schollwöck, Rev. Mod. Phys. **77**, 259 (2005).